AMYGDALA $z \mapsto z^2+c$

A Newsletter of Fractals & $\mathcal{M}$ (the Mandelbrot Set)

Issue #33-34
October 1994

In This Issue...

The Primal Heterotope presents a remarkable graphic journey, starting from the Mandelbrot set and ending at the quasi-Mandelbrot set associated with $z \to z^3 + c$. On the yellow brick road between them, we encounter strange and wonderful beings, some beautiful, some grotesque.

Sound and Ceramics reports on Bart Lynch's efforts to generate pleasing pottery from pleasing sounds, and *Iterations on Clay Pots* raises the question of extending these ideas to fractal processes.

The Mandelbrot Set Chaosometer gives a proposed measure of the amount of chaos associated with the iteration track of a given point in the plane, and discusses how well it works as a detector of chaos in Mandelbrot calculations.

1/f Noise discusses a type of fractal noise which has proved to be quite useful in modelling certain random processes, and presents an algorithm for generating 1/f noise.

Quicksilver Starship discusses a novel idea for drastically decreasing the compute time for generating a video or movie of zooming/panning in the Mandelbrot set.

Quaternion Square Root derives a formula for the square root of a quaternion.

The Primal Heterotope

—Rollo Silver

A couple of years ago, I started to wonder how to deform the quadratic Mandelbrot set (defined by $z \leftarrow z^2 + c$) into the cubic Mandelbrot set ($z \leftarrow z^3 + c$). Could that be done? How? What would it look like?

The topologists call a continuous deformation of one figure into another a *homotopy;* if such a deformation exists, the figures are *homotopic,* and topologically equivalent.

Since the quadratic $\mathcal{M}$-set is connected, while the cubic $\mathcal{M}$-set isn't, they aren't topologically equivalent, hence they aren't homotopic. A deformation of the one into the other may exist, but it can't be continuous, and can't be a homotopy. I decided to call the thing I was looking for a *heterotopy.*

My explorations ended up with the one-parameter family of Mandelbrot sets M_t associated with the

CONTENTS

polynomials $P_t(z) = (1-t)z^2 + tz^3 + c$ $(0 \le t \le 1)$, a heterotopy, or non-continuous deformation of the quadratic Mandelbrot set M_0 into the cubic set M_1.

I call this particular heterotopy the *primal* one because it is the simplest one I can think of: the most primordial one. Simple though it is, it is filled with strange and marvelous phenomena. For instance, there are certain singular values of t near which the M_t change character very rapidly — perhaps infinitely rapidly. In hindsight I might have expected that. Since the deformation can't be continuous, but *tries* to be, there must be critical points at which the discontinuity expresses itself in no uncertain terms.

In his article *The Three-dimensional Mandelbrot Set* (*Algorithm* issue 3.3, pages 20-21), Earl F. Glynn discussed a heterotopy based on the one-parameter family of non-polynomial functions $z \leftarrow z^a + c$, for $1 \le a \le 3$. This approach produces an interesting family of images, but is less simple than the polynomial approach. For one thing, the functions $z^a + c$ are multi-valued, which leads to peculiar slip-planes in their images.

In this article, the figures illustrating the journey from M_0 to M_1 are all greyscale images using one of three "color" schemes; they are all 650 x 489 pixels and have the same escape radius: $R = 10$.

The main sequence consists of a series of views all having the same magnification. There is controversy over the term *magnification* as applied to fractal images. Several people have objected to my attempt to give a precise meaning to the term: the reciprocal of the radius of the largest circle that will fit within the field of view. To avoid controversy I have coined a new term for this reciprocal radius: *suidar*. Most of the images in the main sequence have suidar 0.237 — a value small enough so that all significant portions of every image appear on-screen. Table 1 (page 9) gives the parameters for each of the 31 figures.

With the time-like parameter t linking together an infinity of $\mathcal{M}$-sets, the ensemble of figures achieves a sense of motion and change that transcends the static nature of the individual images.

We start, then, with M_0 — the familiar Mandelbrot set — with t-value 0. Its appearance is familiar — except that with the large value of R, the set is small when the surrounding regions of dwell 0 and 1 are shown.

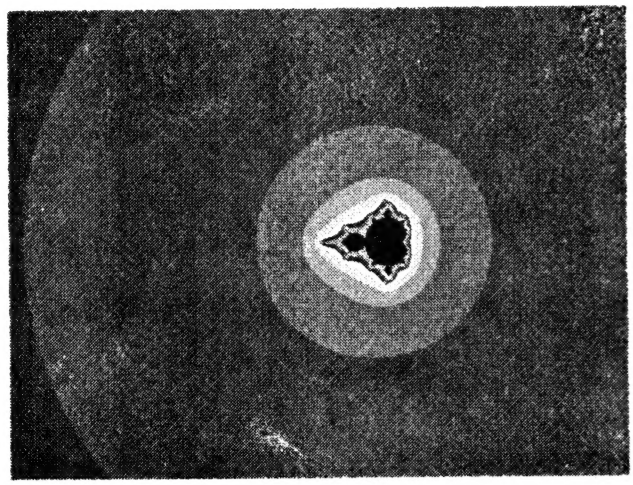

Figure 1: t = 0; suidar = 0.158

We proceed uneventfully from $t = 0$ to $t = 0.072$: the dwell boundaries change shape slightly, the head of the set grows bigger, and the principal buds migrate to the right toward the cusp of the cardioid. All is smooth.

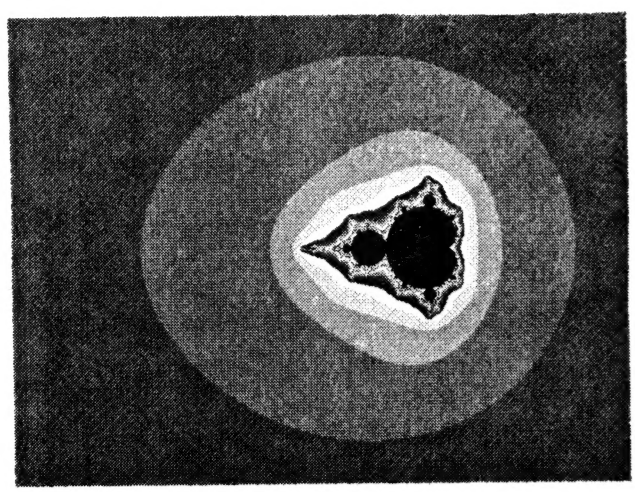

Figure 2: t = 0.072; suidar = 0.237

The cubic term does not intrude topologically until t becomes comparable to $1/R = 0.1$. In fact, something mildly interesting begins to happen for $t = 0.073$, and is clearly manifest by 0.075: A region of dwell 2 breaks through at the critical point -10 and expands eastward. This region is an artifact of

using an escape radius to determine dwells. I do not believe that it would appear with pictures based on the potential.

By $t = 0.08$, the intruder has been joined by cohorts of dwell 3 and 4, and the normal region of dwell 2 is elongating westward toward it.

By $t = 0.10$ (Figure 3) the cubic term has asserted itself aggressively: the two $D = 2$ regions have merged, a real intruder has appeared, and two other lenticulars have appeared north and south.

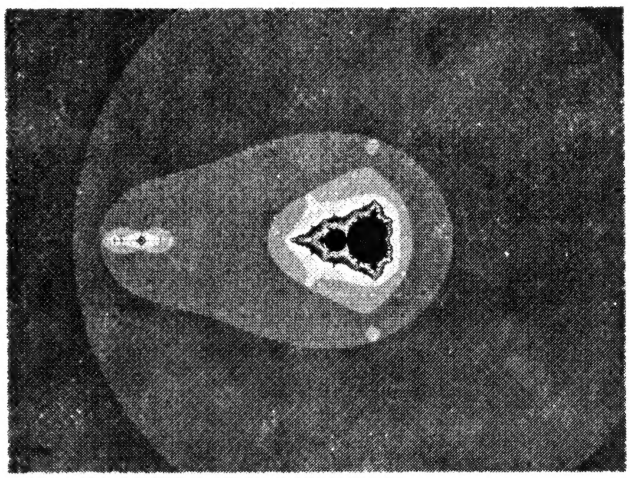

Figure 3: $t = 0.10$ (suidar = 0.13)

Figure 4— a magnified view of the intruder— reveals two facts: that the intruder is genuinely fractal, and that $M_{0.1}$ is disconnected: the contour bounding the region D = 3 is evidently closed, enclosing the midget but not the main set.

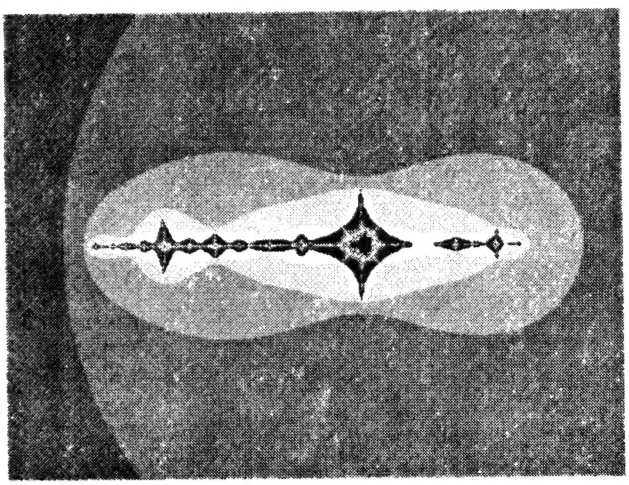

Figure 4: The Intruder (RM = 3.9)

In the next four pictures $t = 0.12$. Figure 5 shows the intruder grown and approaching the main set.

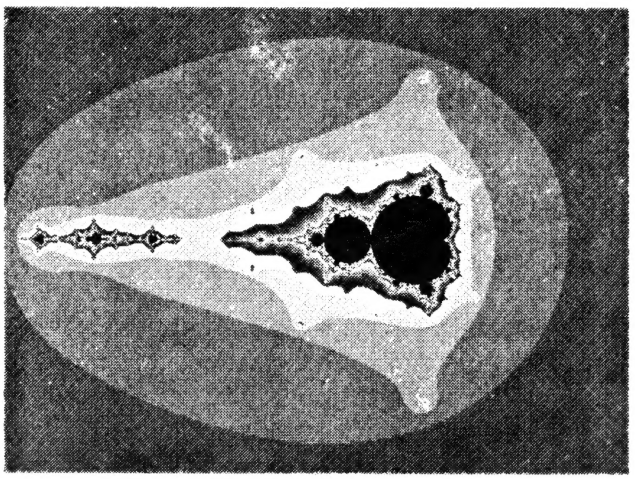

Figure 5: The Intruder Approaches The Set ($t = 0.12$)

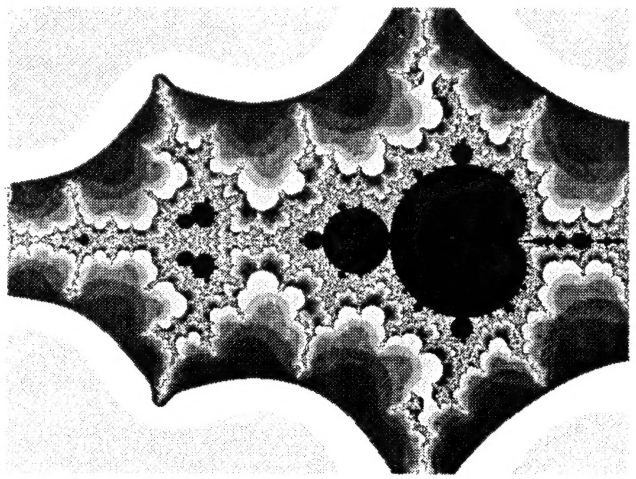

Figure 6: The Intruder Close Up ($t = 0.12$; RM = 14)

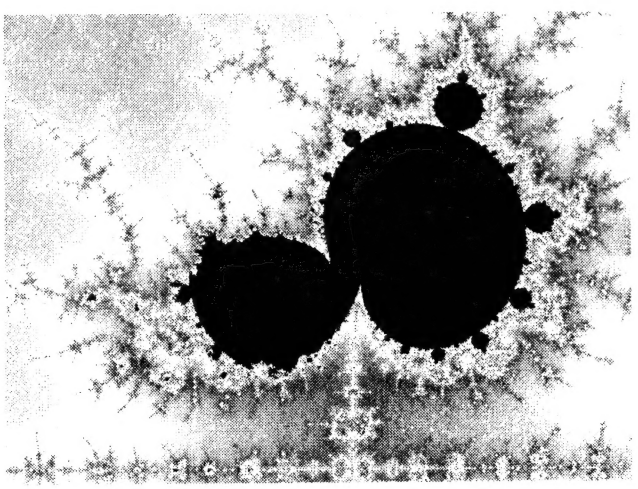

Figure 7: The Ugliest Fractal ($t = 0.12$; RM = 125)

The Ugliest Fractal: A Digression

Now let's digress to get a closer look at the intruder. Figure 6 shows the intruder with magnification 14 relative to Figure 5.

I wonder what that funny double structure to the left looks like? Figure 7 shows its upper half at relative magnification 125.

He's my candidate for the ugliest fractal! But like the toad, ugly and venomous, he wears yet a precious jewel in his head. Figure 8 details the jet ejected downward from the cusp between the two components of the U.F. at relative magnification 950. The jet carries an unusual figure: the aforementioned jewel.

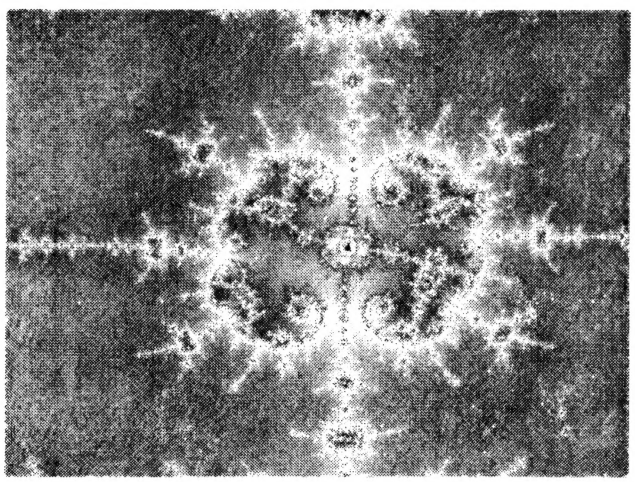

Figure 8: The Jet
(t = 0.12; RM = 950)

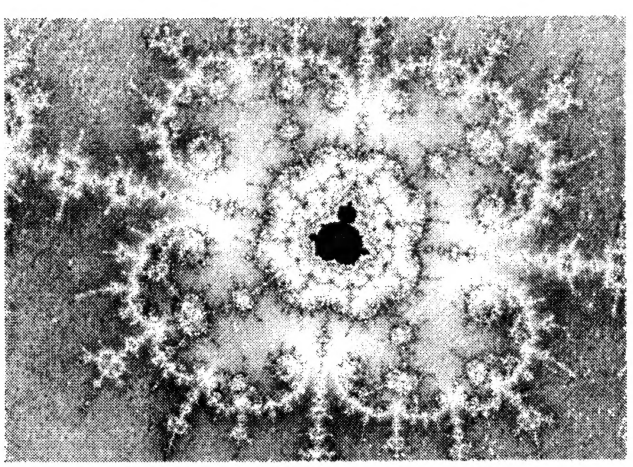

Figure 9: The Jewel
(t = 0.12; RM = 8400)

Figure 9 shows that the jewel in the center of Figure 8 carries a midget in its heart.

Back To The Main Sequence

Let's go back to the main sequence! Continuing from Figure 5 (t = 0.12): as t increases the intruder approaches the main set— what happens as they collide?

Figure 10 shows the intruder approaching the set more closely. A collision is imminent.

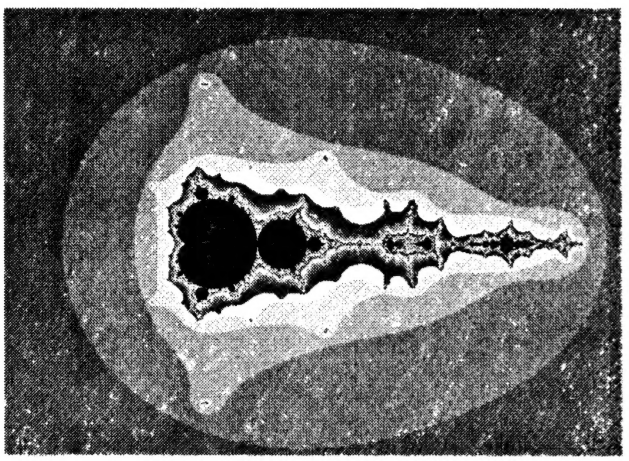

Figure 10: The Intruder Menaces The Set
(t = 0.1258)

Figure 11 shows a magnified view (RM = 7.5) of the area of imminent collision.

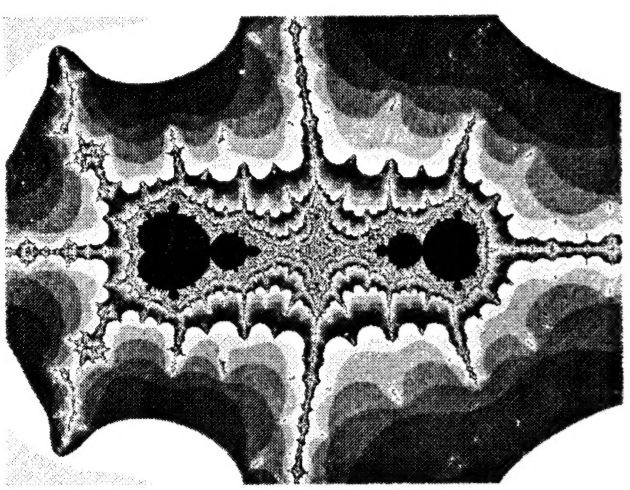

Figure 11: Imminent Collision
(t = 0.1258; RM = 7.5)

The Collision

This is one of the critical points where things change extremely rapidly as t advances. With t = 0.12595 (Figure 12) the collision begins.

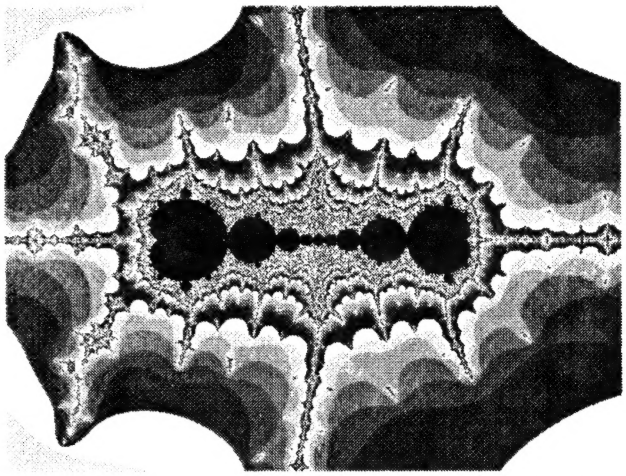

Figure 12: The Collision Begins (t = 0.12595)

The collision proceeds as the two Mandelbrot bodies move together, squeezing the material between them into fewer and larger balls (Figure 13).

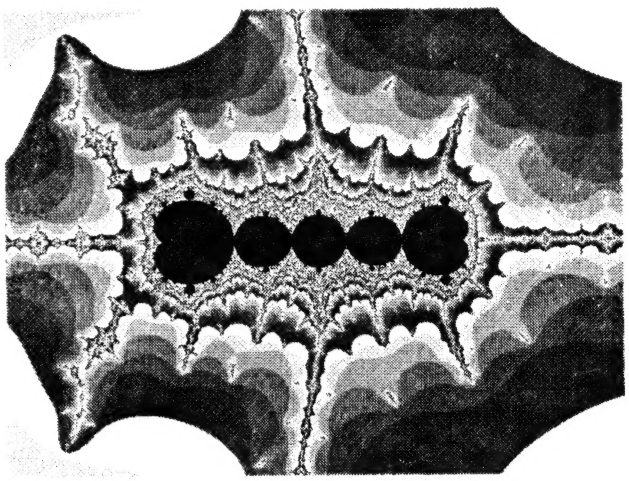

Figure 13: Compression and Inflation (t = 0.126)

As the squeeze continues, the balls coalesce into a single ball, which becomes the common head for the two $\mathcal{M}$-bodies. Small buds appear at the top and bottom of the ball (Figure 14).

Further compression merges the two bodies and the head into a single mass. The buds at top and bottom enlarge (Figures 15). Note how rapidly the figures change with small changes in t.

Now a surprising thing happens (Figure 16). The

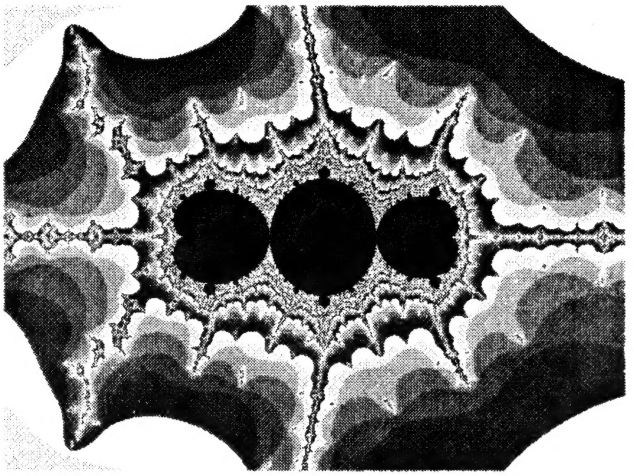

Figure 14: A Common Head (t = 0.1262)

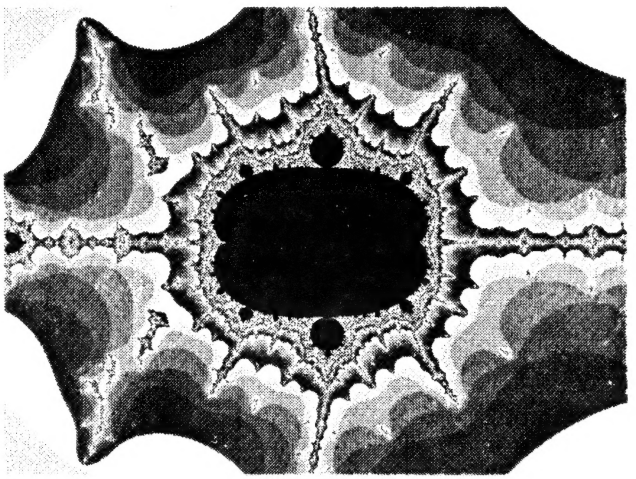

Figure 15: Coalescence (t = 0.1266)

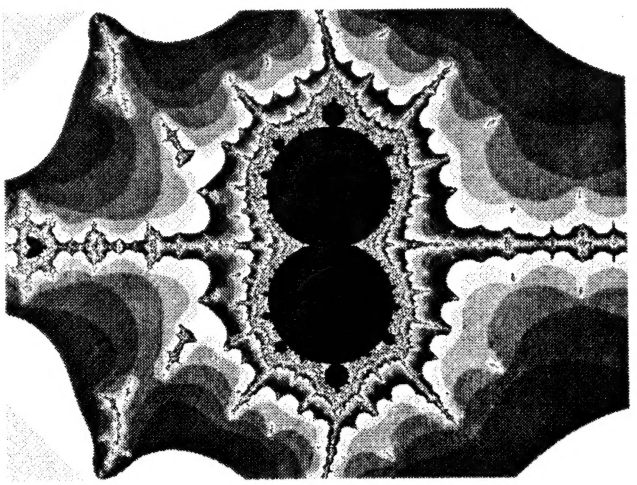

Figure 16: Separation (t = 0.127)

mass is pinched horizontally and separates vertically into two circular bodies. The buds at top and bottom become their heads. Referring back to Figure 11, the paired horizontally opposed midgets have been essentially rotated 90 degrees!

Beyond $t = 0.127$, the midgets separate further and further vertically. In Figure 17 the upper midget is supported on a jet of water, forming a lovely fountain.

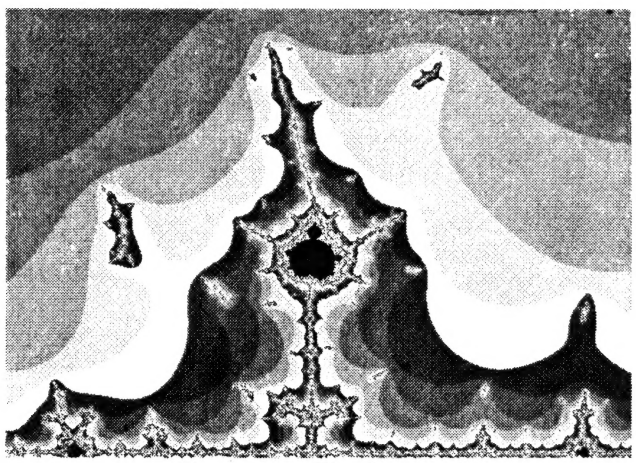

Figure 17: The Fountain ($t = 0.1285$)

We now pull back to get a look at the overall picture (Figure 18).

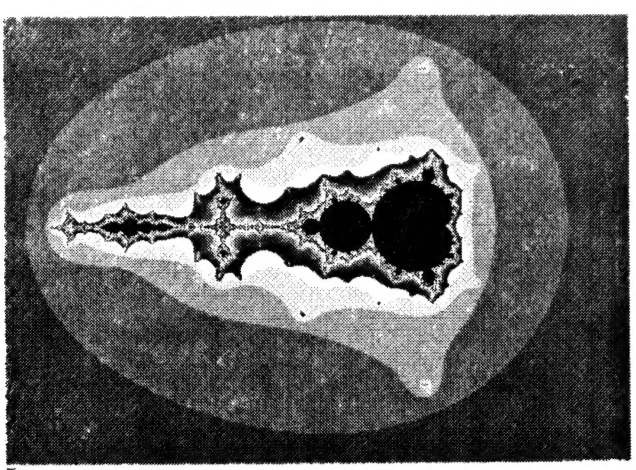

Figure 18: The Fountain in Perspective ($t = 0.1285$)

As t continues to increase, the structure at the left and the original $\mathcal{M}$-set approach a major collision (Figure 19). The collision actually occurs for $t = 0.142$ (Figure 20). Just as for the minor collision shown in Figure 13, a series of more-or-less equally-sized balls forms between the colliders.

As before, further compression coalesces the components (Figure 21).

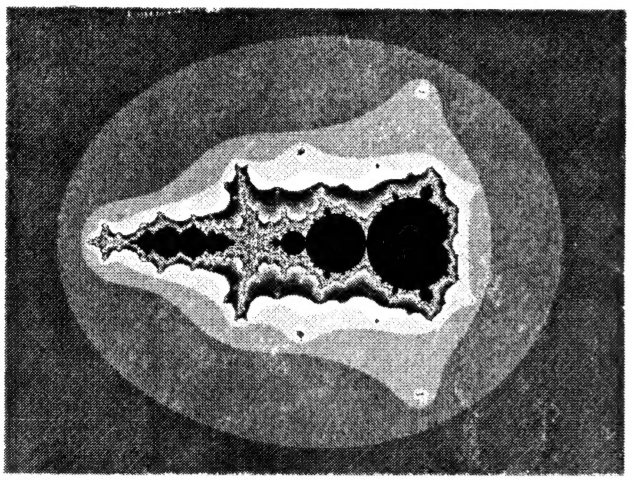

Figure 19: The Major Collision Impends ($t = 0.14$)

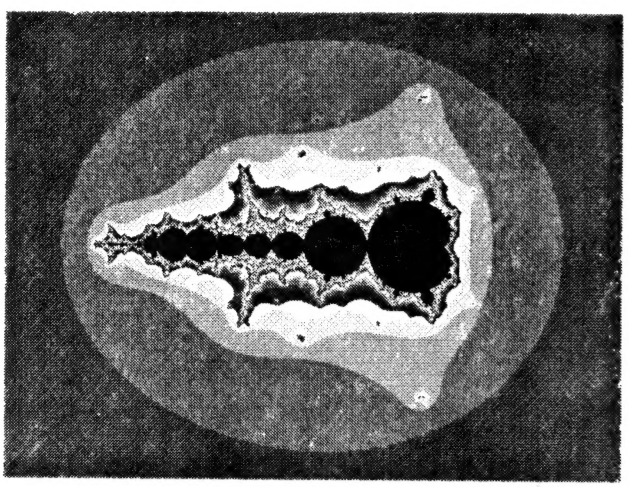

Figure 20: The Major Collision ($t = 0.142$)

By $t = 0.22$ (Figure 22) the coalescence has produced a "bug" with bud-wings above and below.

By $t = 0.28$ (Figure 23) coalescence has resulted in an ovoid with buds similar to the north and south buds of the original $\mathcal{M}$-set M_0 We may consider this the half-way point in the evolution of M_0 into M_1. Examining Figure 23 we might suppose that a vertical cleavage will appear in the north and south buds, converting them into the ones adorning M_1 (Take a peek at Figure 31 on page 9).

A closer look, however (Figure 24: R.M = 7.5), reveals that something odd is going on. A strange rod-like appendage is pushing its way out of the valley between the body of the figure and the bud.

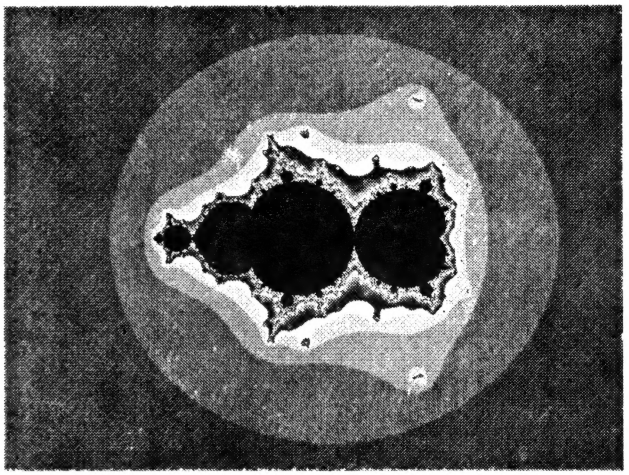

Figure 21: Coalescence (t = 0.17)

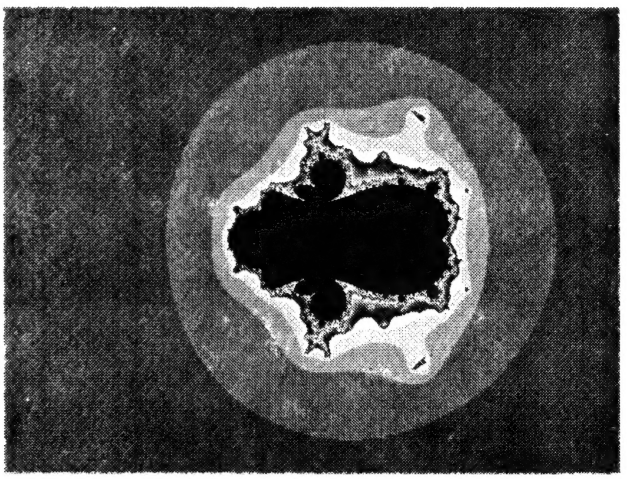

Figure 22: Buds Emerge (t = 0.22)

As t increases further, the appendage thickens and elongates: an absurd obscenity (Figure 25)!

What happens now (starting from Figure 24) is unexpected. The appendage thickens and expands to become the right hand lobe of the head/tail of M_2, while the Mandelbud changes shape to conform.

In Figure 27 (t = 0.40) the hypertrophy of the right lobe continues, and the two lobes change their shape toward enantiomorphism.

With t = 0.50 (Figure 28), symmetry is almost

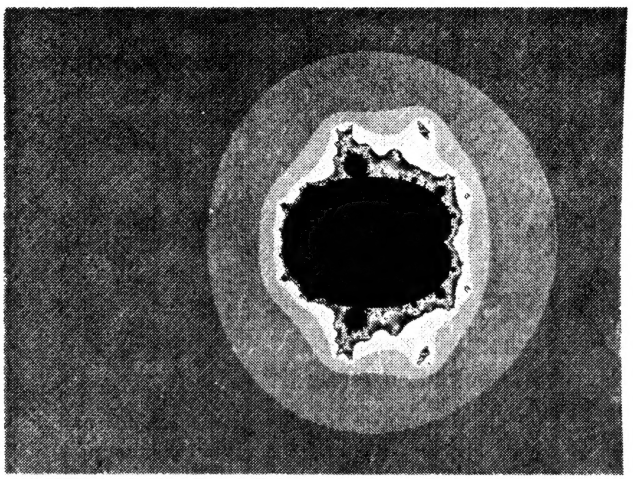

Figure 23: Ovoid With Buds (t = 0.28)

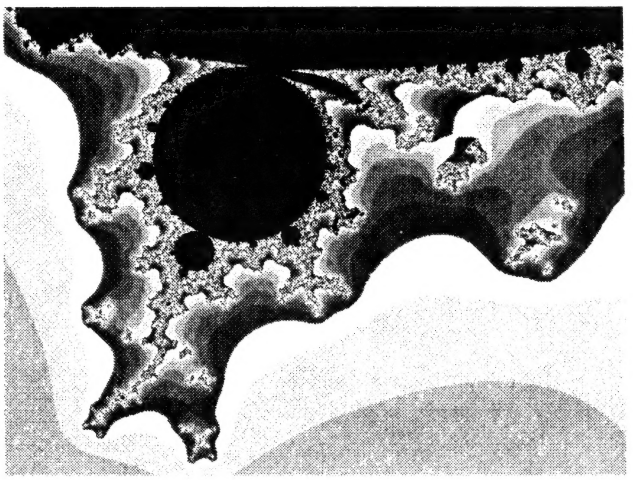

Figure 24: Rod-Like Appendage (t = 0.28; RM = 7.5)

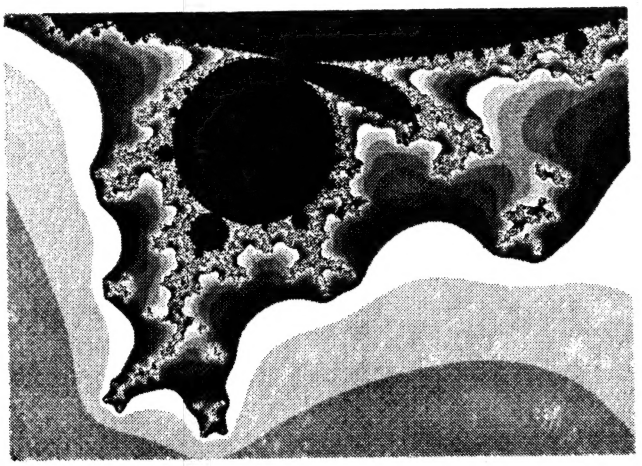

Figure 25: An Ithyphallic Appendage (t = 0.30; RM = 7.5)

achieved.

Before pushing the rest of the way to $t = 1.0$, let's back off and have a look at the big picture (Figure 29).

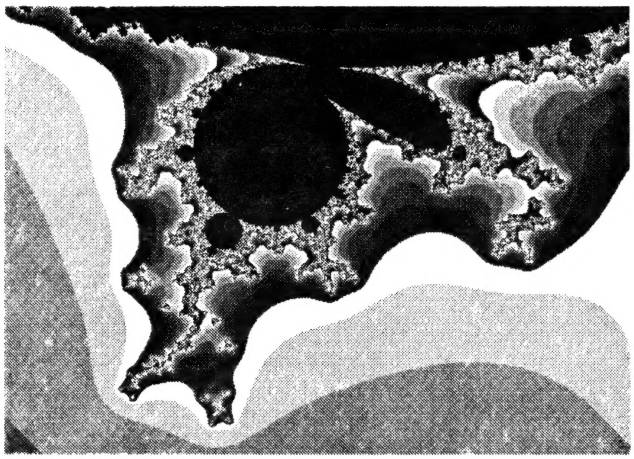

Figure 26: Ithyphallic Hypertrophy
(t = 0.32; RM = 7.5)

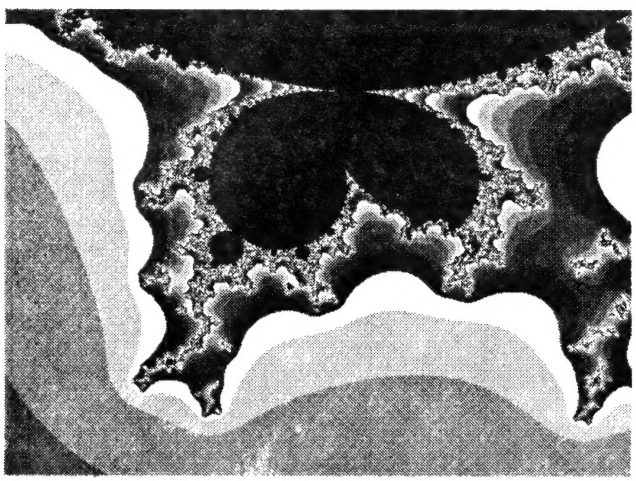

Figure 27: The Enantiomorphic Urge
(t = 0.40; RM = 7.5)

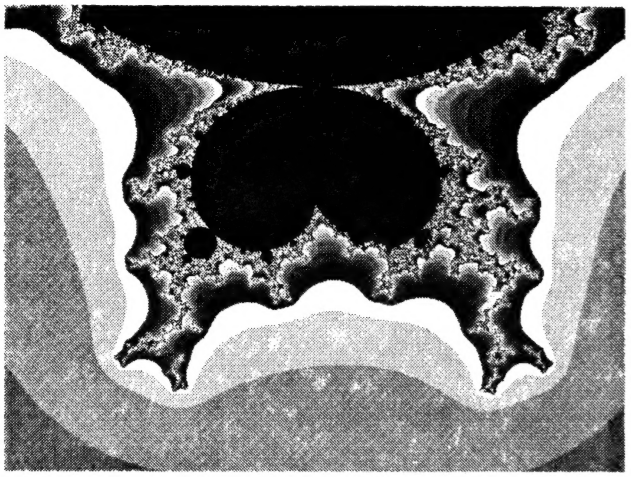

Figure 28: Almost Complete (t = 0.50; RM = 7.5)

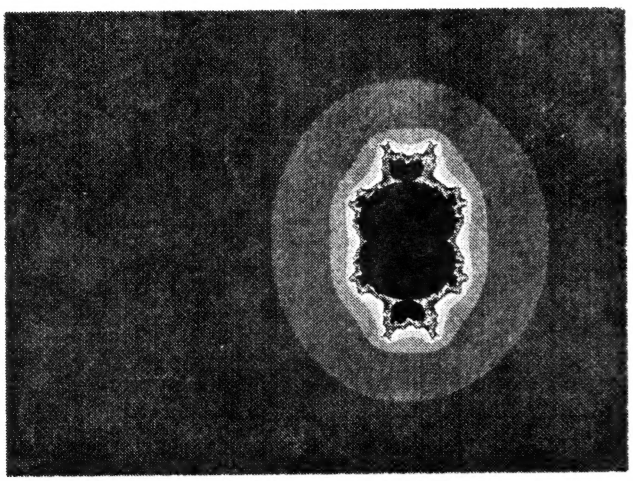

Figure 29: Almost Complete: The Big Picture
(t = 0.50)

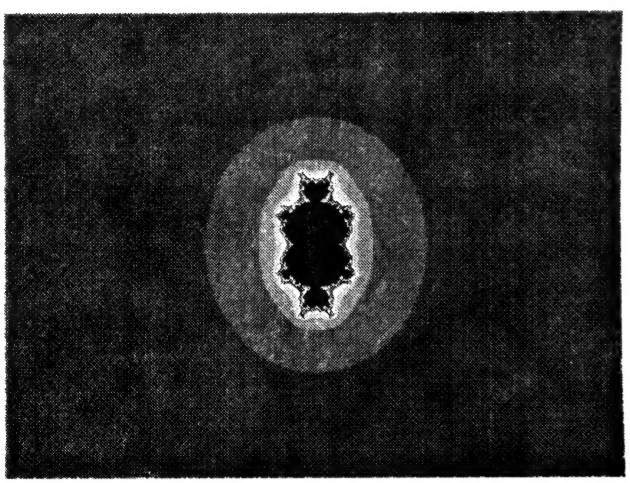

Figure 30:The Cubic Mandelbrot Set, Complete
(t = 1.00)

Figure 30 shows the cubic Mandelbrot set complete, centered in the field of view.

And finally, an enlarged view of the Cubic set's head:

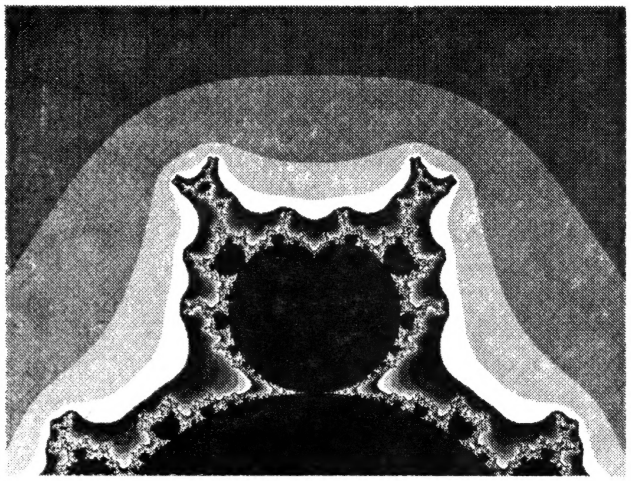

Figure 31:The Cubic Set's Head
(t = 1.00; RM = 7.5)

It's curious that almost all the action takes place in the first half, $0 \le t \le 0.5$. The second half, $0.5 \le t \le 1$, is sedate by comparison.

All the figures were generated using special software written to generate them.

Table 1: Parameters for Figures

FIG (CLUT)	t	suidar	center	max dwell
1 (2)	0.0	0.158	-2.0	500
2 (2)	0.072	0.237	-2.0	1000
3 (2)	0.10	0.130	-2.0	1000
4 (2)	0.10	0.923	-7.940	1000
5 (2)	0.12	0.237	-2.0	1500
6 (2)	0.12	3.37	-6.131	3000
7 (3)	0.12	30.1	-6.292+0031i	3000
8 (3)	0.12	224.	-6.2878+ 0.0064i	4000
9 (3)	0.12	1980.	-6.28734+ 0.00640i	3100
10 (2)	0.1258	0.237	-2.0	2000
11 (2)	0.1258	1.78	-3.753	2600
12 (2)	0.12595	1.78	-3.753	3100
13 (2)	0.126	1.78	-3.753	4000
14 (2)	0.1262	1.78	-3.753	3000
15 (2)	0.1266	1.78	-3.753	3000

Table 1: Parameters for Figures (Continued)

FIG (CLUT)	t	suidar	center	max dwell
16 (2)	0.127	1.78	-3.753	3000
17 (4)	0.1285	1.78	-3.660+0.548i	3000
18 (2)	0.1285	0.237	-2.0	3000
19 (2)	0.14	0.237	-2.0	3000
20 (2)	0.142	0.237	-2.0	4000
21 (2)	0.17	0.237	-2.0	2000
22 (2)	0.22	0.237	-2.0	2000
23 (2)	0.28	0.237	-2.0	2000
24 (2)	0.28	1.78	-1.093-1.591i	500
25 (2)	0.30	1.78	-1.011-1.591i	500
26 (2)	0.32	1.78	-0.950-1.575i	500
27 (2)	0.40	1.78	-0.663-1.539i	500
28 (2)	0.50	1.78	-0.370-1.446i	2000
29 (2)	0.50	0.237	-2	2000
30 (2)	1.00	0.237	0	2000
31 (2)	1.00	1.78	1.132i	500

Sound and Ceramics

Bart Lynch

Reprinted from LEONARDO Electronic News

In architecture, natural harmonies occur in Renaissance structures. Harmonic relations of form and space were often based on the golden section and the ratios therein. These same ratios occur in the growth patterns of flowers, fish, and other components of nature. I am currently concerned with understanding why these ratios occur and why they are pleasing to us.

I have been translating sounds to three dimensional pottery using several computer programs in order to see if pleasing sounds make pleasing pottery and vice versa.[1] Using the sound program SOUND EDIT PRO, I can get a visual representation of a sound that is time dependent. That visual is saved as a picture and imported to SWIVEL 3-D where the sound form can be lathed to resemble pottery and used as a template to create actual

1. This work was developed at Deep Creek School in conceptual collaboration with Dan Collins.

ceramic works. Using these programs, I have also been animating the figures so that on the computer screen, the pottery forms dialogue with the sounds that created them. I see these processes as data gathering exercises that help me to understand the nature of the harmonic relations so that I will be able to use them more effectively in the future.

Iterations on Clay Pots

Stewart Dickson

I have just read Bart Lynch's piece, *Sound and Ceramics,* in LEONARDO Electronic News 3(7) (July 15, 1993). This is a very cool piece, on levels which go quite a bit deeper than he described in his article, I think.

What he is describing is an iterative procedure in which he is translating a physical, 3D object (a clay pot, thrown on a potter's wheel) into an abstract representation. He is "sounding" or "ringing" the object, recording this event and creating an alternate, spatial abstract representation of the object: A graph, presumably a frequency spectrum(?) (he did not say precisely what graph he produced on SOUND EDIT PRO). Wait a minute, on reading more closely, he says, "...that is time dependent." This is merely an amplitude envelope, then. A pity.

At any rate, he then takes the sound envelope graph and uses it as a contour template for throwing a new pot.

If he were to make frequency spectrum pictures, he would be translating the event into the complex phase plane and then we could compare the procedure to those like computing the Mandelbrot set. I think that were Bart Lynch to approach it in this way, that he could map out the divergence and convergence of his procedure; i.e., he would be finding convergent and divergent lathed shapes.

I will refer this to some experts in the field (FRACL) and see what they say. I'm sure the procedure could be simulated. I think the acoustical mechanics of a lathed shape are well known. The question is mainly what kind of graphs will produce convergent sound-producing shapes. I think we can fiddle with the mapping a little until we find something that can produce regions of convergence amid a field of divergent shapes. One can imagine that convergent shapes could be analogous to some kind of purity or "music of the spheres".

Please let me know your response to these ideas. I will compile all responses I receive.

Stewart Dickson
The Post Group
6335 Homewood Avenue
Los Angeles, CA 90028
Phone: (213)462-2300 X 832
FAX: (213)464-1953
Internet: tpg!dickson@rhythm.com

The Mandelbrot Set Chaosometer

—Jay Hill

Those of you who have followed my e-mail posts about the area of the $\mathcal{M}$-set and related computations will have noticed the recurrent theme of how to avoid long computations by early identification of three classes of orbits for the $z \leftarrow z^2 + c$ iteration. These are the *escapers, periodics* and *chaotics.* The sci.fractals.FAQ (Frequently Asked Questions posted on the Internet sci.fractals newsgroup) states that the Lyapounov exponent can be used to identify chaos. If the Lyapounov exponent λ is positive, then the iteration is chaotic. The exponent is defined as

$$\lambda = \lim_{N\to\infty} \frac{1}{N} \sum_{n=1}^{N} \log_2 \left| \frac{dx_{n+1}}{dx_n} \right|$$

Now for the Mandelbrot Set this is

$$\lambda = \lim_{N\to\infty} \frac{1}{N} \sum_{n=1}^{N} \log_2 |2 z_n| \qquad [1]$$

since $z_{n+1} = z_n^2 + c$. It is not clever to do lots of logs, so I have reworked the formula and use

$$J = \prod_{n=1}^{N} 2|z_n| \qquad [2]$$

Then $\lambda = \dfrac{\ln J}{N \cdot \ln 2}$, but you need only compare J to 1: you have chaos if and only if $J > 1$. If you are

iterating c in the center of a component, J will be equal to or very close to zero. In this case, evaluating the logarithm to get λ results in an error. Using formula [2] saves evaluating the logs in formula [1] and gets the same results. The factor of 2 in [2] tends to keep J of reasonable size during the iteration.

How well does equation [1] or [2] work as a detector of chaos in Mandelbrot calculations? I have explored this with mixed results. Along the real line, J remains 'undecided' until n is greater than some value, call it k. In or near a periodic component, I find that k is at least equal to the period. For example, in the period 4096 component centered at -1.4011551704444 (in the Feigenbaum sequence approaching -1.401155189092), $J-1$ remains positive most of the time, dropping briefly below zero at $n = 1024$ and 2048. Only after $n > 4096$ does J become very small. But even then it jumps above one a few more times, depending on how close c is to -1.4011551704444. I have traced the Feigenbaum component sequence to that with period 262,144. Now if I were to have used the Chaosometer to cut off computations for chaotic points early, I'd have missed these small high period components.

On the other hand, chaotic points on the real line (with $\lambda = 0.25$, for example) drive J quickly to very large values ($J > 10^{200}$). These can certainly be abandoned as chaotic saving us the trouble of following the iterations to some maximum iteration value, since the iteration will not ever diverge ($-2 > c > -1.401155\ldots$). For these points the test is useful.

The next example I tried was c = complex points on the boundary of the main cardioid. These are either periodic (tangent to a touching bud) or chaotic. I have posted on FRAC-L a list of chaotic c, some of which I tested here. The formula does not work as well as I would like, since $\lim_{N \to \infty}$ is computationally vague. Let's start with a definitely periodic point, $c = 0.25 + 0.5i$. After more than a million iterations, λ approaches zero, mostly from the minus side, but not completely. It occasionally jumps positive for one or two iterations. A nearby chaotic point is $c = 0.2850441472 + 0.4607492096i$. Again, λ approaches zero, but now mostly from the positive side, but even after more than a million iterations, it still drops to negative (hinting at periodic).

It would appear that λ for c on the edge of a component will approach zero in a jerky manner, and the test is not very useful. The test will work well for points on filaments, points far away from component edges.

I recommend it for use in Mandelbrot calculations along with period detection and other tests and devices. Since the only filament we know well is the real line, the test should at least be used when c is pure real.

Implementing a 1/f Noise Algorithm

Gabriel Landini

Many computer simulations are based on random white noise generators provided in program libraries. Voss and Clarke [Vos88] demonstrated that there is another type of random fluctuation almost universally present: *1/f noise*, which has a spectral density which is proportional to the reciprocal of the frequency — a random fractal noise.

Although 1/f noise occurs commonly, there is no clear explanation of how it arises. Some believe that 1/f noise arises when processes change from chaotic to periodic behavior. Others attribute it to multiple additive or multiplicative random processes [Wes89].

Sources of 1/f fluctuation include the annual floods of the Nile river, sunspot activity, the fluctuations of electric current in thin metal sheets, cardiac electrical activity, stock exchange prices, amplitude fluctuations in human speech, and pitch fluctuations in music.

In many cases computer simulations would be more realistic using 1/f noise rather than white noise. In *The Science of Fractal Images*, Voss gives a method for generating 1/f noise using the inverse fast Fourier transform (IFFT) which requires extensive computation.

I implemented an algorithm for 1/f noise in Quick-

BASIC which is based on an idea of Voss published elsewhere [Gar78] in which the values of random generators (dice) are added following a binary table of frequencies.

1/f noise possesses a spectral density inverse to frequency: high frequencies, low power. This also means that 1/f noise possesses scaling properties: a 1/f sequence will look statistically similar if we plot the same sequence skipping 1 value, 2 values, 4 values, etc. Although this is true of white noise as well, it is worth trying to see what happens when a one-dimensional random walk or a sine wave are scaled.

The program generates a sequence of length 2^d depending on the number d of 'dice'. The dice generate values from 1 to v, and the data have a Gaussian distribution of values between d and vd with an arithmetic mean $\frac{d+vd}{2}$.

I ran the program 1400 times with 9 dice (length = 512) using values of v = 3, 4, 6, 8, 16, 32, and 64 (200 times each). Each time I calculated the spectral density and its slope using the least squares method. The slope and correlation coefficient of the regression lines of a log-log plot of the spectral density of the 1400 runs did not show differences, so to get a wider range of values it is valid to increase v.

Figure 1 shows the output of 1024 values of the algorithm analyzed with the Fast Fourier Transform. The sampling interval is one second, and there are eight degrees of freedom. A line with slope -1 — ideal 1/f noise — is superimposed for reference.

Another attractive characteristic of 1/f noise is its autocorrelation, which falls between uncorrelated white noise and the short time correlations of Brownian motion.

Figure 2 shows the autocorrelation function of 1/f noise, which decays exponentially.

Further experiments are possible, for example to create a color palette shading from white to black to blue to red, and then plot a sequence of pixels with the color value taken from the 1/f sequence. In this way, the autocorrelation of 1/f noise can be compared to that of white noise, a sine wave, or Brownian motion.

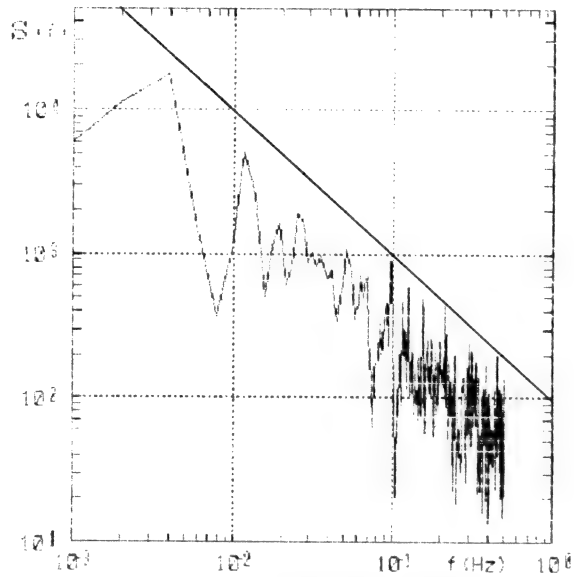

Figure 1 — Spectral Density

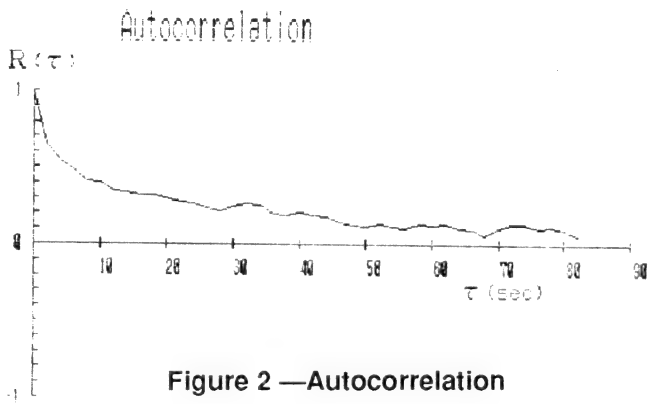

Figure 2 —Autocorrelation

My study of clinical patterns of a buccal disease (periodontal disease) has some interesting theoretical implications [Lan91a].

In another area, I found that 1/f data translated into music produces very pleasant results [Lan91b], as Voss discovered.

References

[Vos88] R. Voss, in *The Science of Fractal Images*, Peitgen and Saupe, eds. Springer-Verlag, New York (1988). Pages 21-70.

[Wes89] B.J. West and M.F. Schlesinger. *On the ubiquity of 1/f noise.* Int. J. Modern Physics B,

3(6), (1989). Pages 795-819.

[Gar78] M. Gardner. *White and Brown Music, Fractal Curves, and One-over-f Noise.* Scientific American, April 1978. Pages 16-31.

[Lan91a] G. Landini. *A Fractal Model of Periodontal Breakdown in Periodontal Disease.* J Period Res, 26 (1991). Pages 176-179.

[Lan91b] Landini, G. *Algo de Ritmo* (letter), Algorithm, 2(3) (1991). Pages 2-3.

Quicksilver Starship

— *Rollo Silver*

Introduction

Making a fractal movie or video of significant length requires a huge amount of computation. The successive frames of the production are usually computed independently, although there is clearly a great deal of frame-to-frame redundancy.

I present here a sketch of an algorithm — which I call the *Quicksilver Starship algorithm,* or QSA — which harnesses that interframe redundancy to provide enormous reductions in compute time.

A Reversal

Usually one thinks of a fractal image as a mapping of a region in the complex plane onto the rectangular pixel array of a monitor screen. By reversing this view, considering the mapping to go the other way— from the pixel array to the complex plane— we can get a significantly new insight into the process.

Concept

Abstractly speaking, a fractal image is composed by computing the dwell value $\Delta(P)$ — a non-negative integer — for each point P in an $m \times n$ rectangular array of equally spaced points, and then coloring the corresponding pixels of an $m \times n$ color monitor screen according to a color mapping table or function $\Gamma(n)$ which maps non-negative integers into colors.

In many cases — all those of interest to me, for instance — the time required to compute $\Delta(P)$, is proportional to the value $\Delta(P)$ itself.

The application of QSA is not in generating a single fractal image, but in generating a whole series of closely related images displayed at high-speed as a series of *frames* to create the illusion of continuous motion through a fractal space.

It's fine if we have a computer powerful enough to do the necessary calculations quickly enough; otherwise we have a basic problem: How can we make use of the information computed in one image of the series to reduce the complexity of computing the next? We need a technique which will bridge the gap between the brute force capacity of our computer and our requirements.

I have gone through a series of models of decreasing complexity, arriving at last at one which is breathtakingly simple. All the models involve the idea of separating one set of points in the complex plane — those whose dwell is computed — from another set: the points corresponding to displayed pixels. Let's call the former points *stars* and the latter *punkts.* For example, the figure below shows a set of stars lying in one rectangular array, and a set of punkts (represented by disks) lying in another:

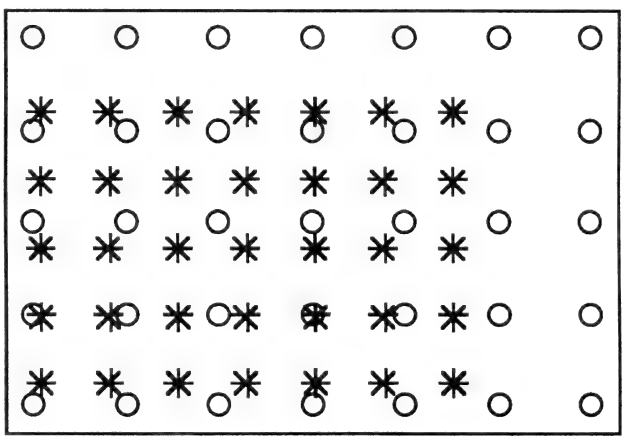

Figure 1 — Stars and Punkts

The "breathtakingly simple" idea is to compute the color value γ at a punkt P using the dwell value at the nearest star S: $\gamma(P) = \Gamma(\Delta(S))$, where Γ and Δ are the color mapping function and dwell function described above.

In order for this to work, we have to maintain a relationship between the two arrays. We can't just

compute an array of stars (say the punkts in the first frame) once and for all, and then use them for all our punkt arrays. The problem is that there may not be a star sufficiently close to each punkt.

Let's make precise what we mean by "sufficiently close". Let's define the *mesh* μ of a punkt array to be the distance between adjacent punkts. We then require that the distance $\delta(P, S)$ between a punkt P and the nearest star S to it be no more than half the mesh:

$$\delta(P, S) \leq \mu/2 \qquad [4]$$

where we define the distance not as the usual Euclidean distance $\sqrt{(x_P - x_S)^2 + (y_P - y_S)^2}$, but as the "Hausdorff metric":

$$\delta(P, S) = max(|x_P - x_S|, |y_P - y_S|) \qquad [5]$$

Thus each punkt has a square neighborhood or *box* around it of "diameter" μ (Figure 2, below).

Stars whose centers are inside the box are near enough to the punkt; stars outside are not.

The idea, then, is that we only need to compute a star dwell when there is no star sufficiently close to the punkt at the center of a box. To keep things simple, we'll keep the stars organized into a rectangular array as much as possible.

If the box around a punkt has no star in it, we compute the dwell of a point within the box, turning it into a star. We simply choose the point which is the center of the square.

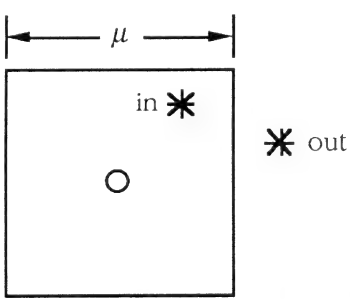

Figure 2 — Hausdorff neighborhood of a punkt

We're now ready for an example.

Example: Zooming Straight In

We start with a 7×5 array Π_0 of punkts, and compute the dwells for a 7×5 array Σ_0 of stars aligned with Π_0 (Figure 3).

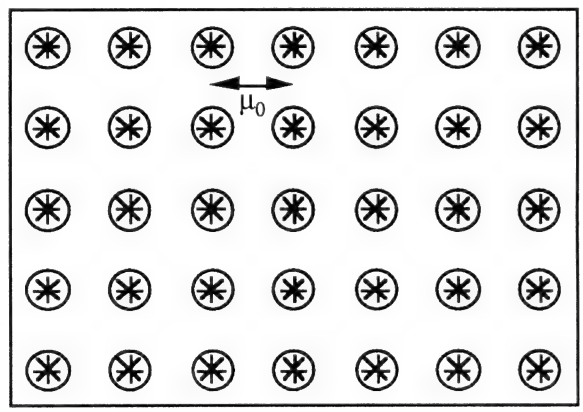

Figure 3— Initial Array of Punkts and Stars

We define μ_0 to be the mesh μ of the initial punkt array Π_0.

Let's see what happens as we zoom in to the central half of the hull of this figure (Figure 4), taking 24 frames to do so. This rate — 24 frames to halve the frame size — seems like a reasonable maximum speed.

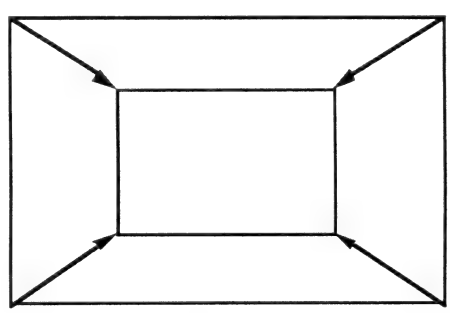

Figure 4 — Zooming In

Let's make the series of frame sizes a geometric series, so the ratio of sizes of any two successive frames is $\sqrt[24]{2} \approx 1.0293$. Table 1 (later on) gives the sizes of the successive frames relative to frame zero, the first one. Let's retain the stars of the original figure, but replace the punkts by their square neighborhoods (*boxes*) of diameter μ. The initial

situation is shown in Frame 0.

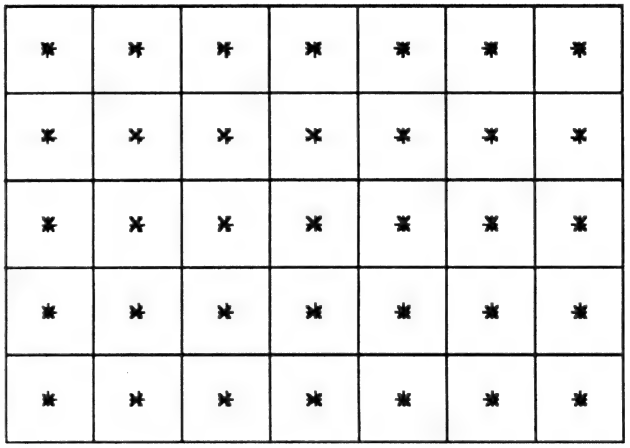

Frame 0— Initial Configuration

Frame 6 shows the state of affairs after six zoom-in steps. The punkt array has shrunk to 0.8409 of its original size: the grey circles cover stars that have just passed outside the frame, and the circled stars have just been created at the centers of empty boxes.

Frame 6b shows the frame after the escaped stars and the circles around the new stars have been removed.

Frame 8 shows the state of affairs after zoom step 8. The punkt array has shrunk to 0.7937 of its original size. The grey circles cover stars which have moved outside all the boxes. In addition the 16 circled stars have been created to fill empty boxes. Frame 8b shows frame 8 as it actually appears.

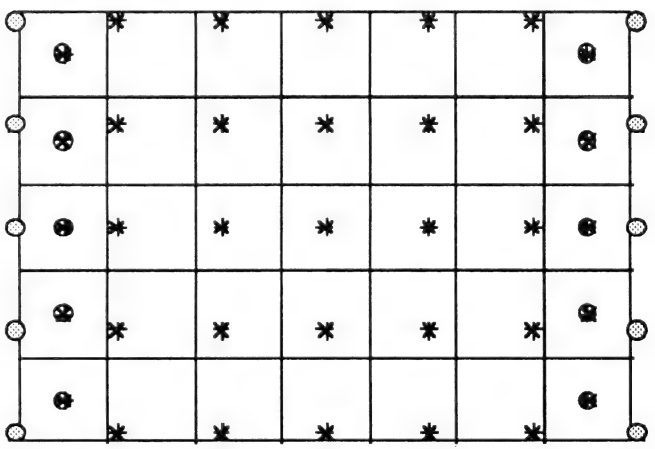

Frame 6 — After Six Steps, showing escaped stars and new stars

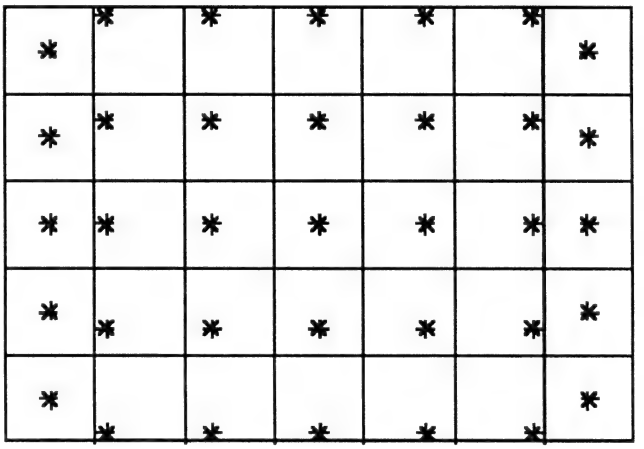

Frame 6b — stars and boxes

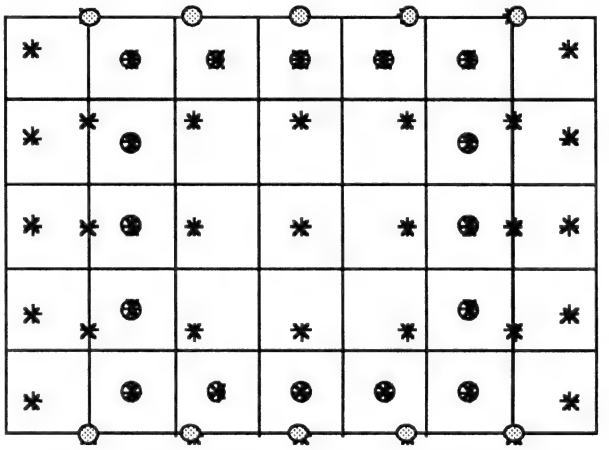

Frame 8 — After eight steps, with escaped stars and new stars

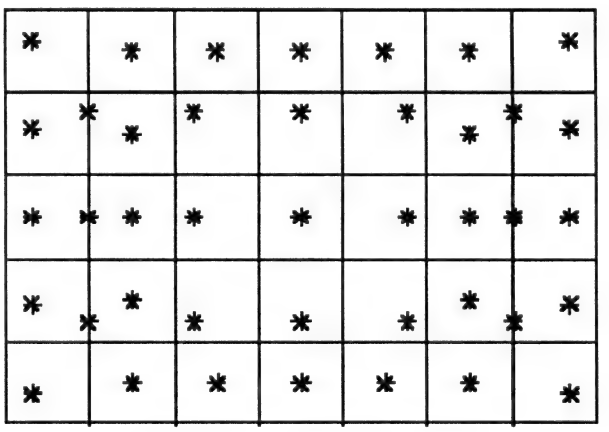

Frame 8b — stars and boxes

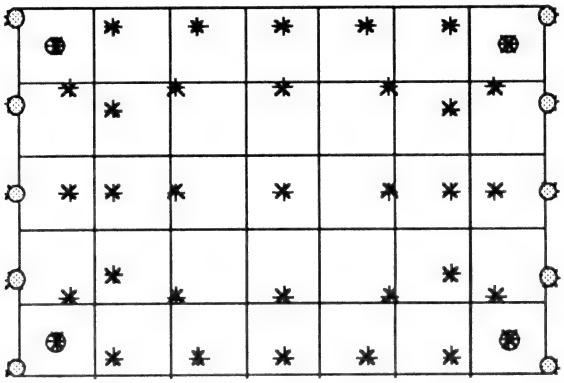

Frame 12 — After 12 steps, with escaped stars and new stars

Frames 12 and 12b show the state of affairs after zoom step 12. The punkt array has shrunk to 0.7071 of its original size. Ten stars have moved out of the frame, and four stars have been added at the centers of empty squares.

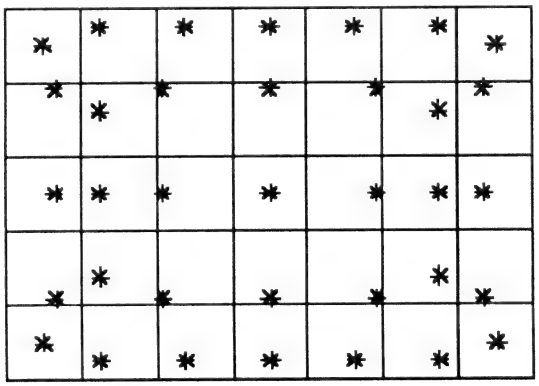

Frame 12b — stars and boxes

Frames 14 and 14b show the state of affairs after zoom step 14. The box array has shrunk to 0.6674 of its original size. Six stars have been added at the centers of empty boxes.

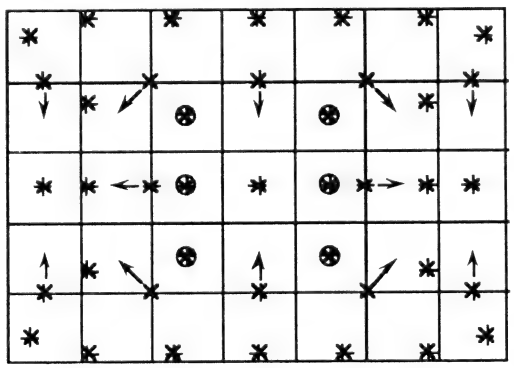

Frame 14 with new stars

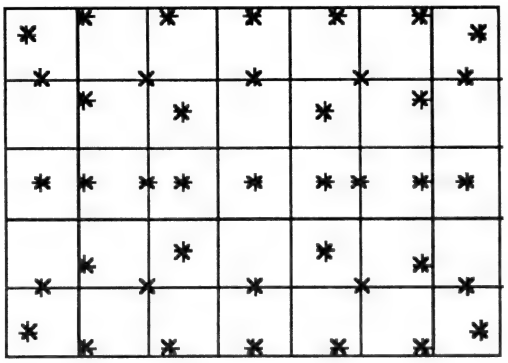

Frame 14b — Stars and boxes

The stars which appear to be on the boundary between two boxes, or in the common vertex of four boxes, are actually not: the arrows indicate which box such a star is really in.

Instead of continuing to show the details of stars lost outside the shrinking box array and new stars created to occupy newly empty boxes for the successive frames, we summarize the situation in the following table, and then show the final frame: #24. The table has entries for only those frames which have significant activity, i.e. which have either lost stars or have gotten new stars created in them.

Table 1 — Frames with significant activity

#	Scale Factor	Lost stars	New stars
0	1.000	0	35
6	0.8409	10	10
8	0.7937	10	16
12	0.7071	10	4
14	0.6674	0	6
15	0.6484	0	6
16	0.6300	10	8
17	0.6120	10	8
18	0.5946	4	0
20	0.5612	6	4
21	0.5453	4	0
23	0.5147	0	4
24	0.5000	4	8

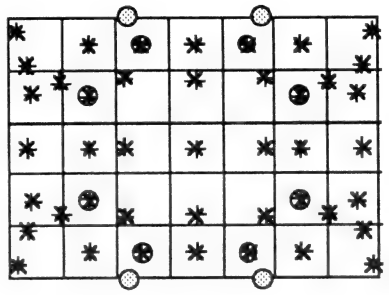

Frame 24 — lost stars and new stars

Let's sum up. If we did not take advantage of the frame-to-frame redundancy of the process, we would have computed 35 stars for each of the 24 frames of the zoom shot after the first: a total of 840 stars. This requires a computer having star-compute power of 35 stars/frame.

Applying QSA, we need only compute 74 stars for the 24 frames, requiring star-compute power of 3.08 star/frame: an elevenfold reduction.

Practical Situations

In practice we shouldn't take the speedup factor of eleven too seriously: it will be affected by the size of the punkt array, the zoom rate, and panning.

I'd expect the speedup factor to increase with increasing array size: In proportion to the linear dimension of the array, I would suggest, since for an $m \times n$ array, the number of stars is proportional to mn, while the number of stars lost per frame should be proportional to the number of boundary pixels: $2(m+n-4)$.

I'd expect the speedup factor to decrease with increasing zoom rate. If we define the "half-life" τ to be the number of frames computed between one frame and the following frame half its size ($\tau = 24$ for the example given), I'd expect the speedup factor to be proportional to τ.

I'd expect the speedup factor to decrease with increasing pan rate. If we define the pan-time to be the number of frames computed during the time it takes for a star to move from one edge of the punkt-rectangle to the opposite edge, I'd expect the speedup factor to be proportional to the pan-time.

For example, if we produce a fractal zoom movie which runs at 24 frames/second, and we have a rectangle of 640×480 pixels, and we zoom in toward the frame center at a rate which halves the frame-size every two seconds, I would expect a speedup factor of about 2,000!

If such staggering speedup factors prove in fact to be the case, we will find ourselves at the dawn of a new era, in which we can produce not only pre-computed, canned displays on a personal computer, but also undertake real-time journeys through fractal space, controlled by a human operator using a joystick and throttle!

Implementation

If you are interested in implementing QSA, you should contact me if you need help with details of the algorithm or data structures to support it. In any case, we should discuss the conditions of your implementation (e.g. freeware, shareware, commercial application), and arrange for permission for you to use my algorithm.

Complex Inverse Trig Functions

Kerry Mitchell

On Compuserve, a question came up about inverse trig functions of complex variables. These formulas, from *Complex Variables and Applications* by R.V. Churchill and J.W. Brown (McGraw-Hill, 1984), may be useful to die-hard fractal freaks such as myself.

$$\operatorname{asin} z = -i \log\left(iz + \sqrt{1 - z^2}\right)$$

$$\operatorname{acos} z = -i \log\left(z + i\sqrt{1 - z^2}\right)$$

$$\operatorname{atan} z = \frac{i}{2} \log \frac{i + z}{i - z}$$

$$\operatorname{asinh} z = \log\left(z + \sqrt{z^2 + 1}\right)$$

$$\operatorname{acosh} z = \log\left(z + \sqrt{z^2 - 1}\right)$$

$$\operatorname{atanh} z = \frac{i}{2} \log \frac{1 + z}{1 - z}$$

RS adds:

For purposes of calculation, these formulas must be reduced to functions of a real variable and simple complex arithmetic, so we need the following formulas as well:

$$\sqrt{z} = \pm\sqrt{r}\left(\cos\frac{\theta}{2} + i\sin\frac{\theta}{2}\right),$$

$$\log z = \log r + i(\theta + 2\pi n),$$
$$n = \ldots, -1, 0, 1, 2, \ldots$$

where $r = \sqrt{x^2 + y^2}$, $\theta = \text{atan}\frac{y}{x}$ and of course $z = x + iy$.

Note that the square root and log functions are multi-valued: $\sqrt{z}$ has two values, while $\log z$ has an infinity of values, one for each integer value of n. Which of the multi-values to use when calculating is a deep question, beyond the scope of this note. For some insight into this conundrum see the article *Bifurcations,* in Amygdala #3.

For those readers who may have some difficulty it seeing how to turn the math into code, here's how the first function might be implemented:

$$\text{asin}\, z = -i\log(iz + \sqrt{1 - z^2})$$

$$\log z = \log r + i(\theta + 2\pi n)$$

$$\sqrt{z} = \pm\sqrt{r}\left(\cos\frac{\theta}{2} + i\sin\frac{\theta}{2}\right)$$

Here's code to compute u and v given x and y, where $u + iv = \text{asin}(x + iy)$. I'll assume n to be externally defined for use in the log function. *pi* is the constant $\pi = 3.14\ldots$.

```
x1 = 1 - x^2 + y^2
y1 = -2*x*y
q = sqrt(sqrt(x1^2 + y1^2))
t = atan(y1/x1)/2
x2 = -y + q*cos(t)
y2 = x + q*sin(t)
u = atan(y2/x2) + 2*pi*n
v = -log(x2^2 + y2^2)/2
```

Book and CD Reviews

"Fractal Fantasies" by Lee H. Skinner (A CD ROM)

A review by John Jones

This is not the first time I've seen fractal images, but it is the first time I've used a CD-ROM. The first thing I noticed was that a CD-ROM holds a *lot* of data — there are over 2,000 images on the disk. And each image actually appears three times — in 1024-by-768 resolution, 640-by-480 resolution, and 16-to-a-screen thumbnail resolution. I viewed the ROM on a PC with a VGA video card, so I looked at the 640-by-480 images, then transferred the high-resolution versions of a few of my favorites to a SparcStation for detailed examination.

But who would want 2,000+ fractal images on CD-ROM? Only a hard-core fractal enthusiast. And such enthusiasts often prefer to create their own images.

Fortunately, the CD also includes source code for FractInt. So it doesn't just offer a passive viewing experience; the images provide a guide to the enormous range of possibilities in FractInt itself, and may inspire the viewer to explore independently.

The images don't provide a map to the worlds reachable via FractInt; rather, they are snapshots from one person's extensive wanderings through those worlds. And on the whole they are snapshots, not Ansel Adams masterpieces. There are masterpieces on the disk: I have a list of forty images that are as impressive as anything I've ever seen. EPSCR/1ASPENEP.GIF, for example, is a beautifully composed picture, which reminds me of Escher's *Three Worlds*; RCL10/1THEBLOB has a marvelous color scheme, showing fluid orange pseudopods reaching up under a canopy of fir trees. And there are several hundred others which are sufficiently interesting to make me want to explore the regions that they came from. But perhaps 80% of the images left me cold. This is partly a matter of familiarity — there are whole series of images that have the same texture as the Mandelbrot set, and I found these far less interesting than textures new to me, such as the Kandinskian compositions in the E1E2 subdirectory — and partly a matter of the care that went into crafting each

image — some of the pictures don't seem to have a focus of interest, while others have strangely clashing colors. ZEPE-F/1ZEXPF90.GIF, for example, is pleasing but poorly framed, while PARABLA.GIF is marred by the contrast between juxtaposed areas of blue and orange.

This does not detract from the usefulness of the CD; sometimes a snapshot is enough. And other viewers may find gems among the 80% I'd dismiss.

My most serious complaint about the CD is the difficulty of finding where a particular image came from. Sometimes this is not too difficult — for example, the images in directory CHCO are described as of type FZPPCHCO, and searching the FRACTINT.FRM file of the PROGRAMS subdirectory, I was able to find the corresponding formula. But the images for which I most wanted the source, the beautiful and mysterious images of MBCOMP, had only the tantalizing description 'Mandelbrot Comparison Images', and I still have no idea how to recreate them. Maybe this information is stored in FractInt. But many potential purchasers of the CD may have a computer, like my Sparc, on which FractInt won't compile. So if the slide-show is to stand alone, it would be nice to have this information ready to hand. A hypertext interface might be the best way of doing this.

A second flaw in the CD is the fact that several subdirectories are missing from the 640 image series. In particular, HALLEY, LAMB, LEES3D and LPC are featured at 1024 and in thumbnail resolution, but not at 640. This is a pity, because the 3-D pictures are excellent.

My final peeve is that 'ancestor' is misspelled as 'ancester' throughout.

In summary, I would say that this CD is certainly worth its price. Viewing it has suggested many avenues for further exploration.
— *John Jones*

$35.55 + $5 shipping, from Amygdala.

"Fractals and Chaos in Geology and Geophysics"

A review by Ian Lumb

Fractals and Chaos in Geology and Geophysics, Donald L. Turcotte, Cambridge University Press, 1992 pp x+221. ISBN 0-521-41270-6; QE33.2.M3T87. Price: $54.95 (hard cover).

This book is intended to introduce the reader to the concepts of fractals and chaos in geological and geophysical contexts. Designed to serve the senior-undergraduate level, this text is supplemented by an up-to-date reference list plus glossaries of terms, units and symbols; 15 of the 17 chapters include instructive problems, many of which have solutions listed at the end of the text. Although the text is ideally suited for those well versed in geology and geophysics, it is sufficiently self-contained to be accessible to those from other disciplines.

After a brief introductory chapter, the next seven chapters focus on fractals. In the second chapter, the concept of a fractional dimension is clearly introduced in one, two and three dimensions. The author moves swiftly from a consideration of the fractal dimension of 'classical' fractals, to 'real-world' coastline and topographic data. Although the use of power-law statistics in geology and geophysics predates the fractal concept (B. B. Mandelbrot, 1967), it is instructive to explore a variety of size-frequency distributions using a fragmentation framework provided by fractals. Since fragmentation involves the highly nonlinear process of fracture propagation, and interactions between these fractures of varying scales, a fractal-based description seems to be called for; the models of fragmentation developed in Chapter 3 allow for a discussion of a variety of processes which include explosions/impacts, weathering, and porosity. Starting with the classic Gutenberg-Richter law, fragmentation models are used to illustrate the scale invariance of frequency-size distributions of earthquakes in Chapter 4; the same scale independence of volcanic eruptions closes out this chapter. In the next chapter, the relationship between mean grade and cumulative ore tonnage is illustrated for the production of several economically interesting ores, as well as for oil field production. When fractal distributions are related to probability, one can study the clustering of events in time or space; this is the subject of Chapter 6, where a brief application to seismicity data is considered.

Up to this point, the author indicates that only self-similar fractals have been considered; i.e. those that are statistically similar at different scales, save

for a multiplicative factor. On the other hand, self-affine fractals involve scaling factors raised to a power, and are usually treated with spectral methods. Thus in Chapter 7, the author presents a comprehensive review of fractal-dimension estimation via spectral methods in one and two dimensions; real-word examples include seismic reflection coefficient, topography, and geoid data. Four color plates close off this chapter with illustrations of synthetic topography, plus fractal and roughness parameter characterization of digitized topography. The scale invariance of erosive processes allows for landscape evolution modeling, via spectral methods, in Chapter 8.

In Chapter 9, an introduction to dynamical systems is provided through an analysis of the van der Pol equation; a solid review of the 'classic' logistic map follows in Chapter 10. The author illustrates how the logistic map iteratively evolves as based on different choices of a constant parameter and an initial value; in so doing, fixed points, limit cycles, chaotic behavior, and bifurcations are all well illustrated. Quantification of the degree of chaos, as provided by the Lyapounov exponent, is also explained and illustrated in this same context.

The production of an earthquake involves the formation of a pressure bond between adjacent crustal blocks, which allows for a build up of elastic strain potential energy. Once the potential energy exceeds the strength of the pressure bond, brittle fracture occurs to release the strain, and the potential energy is converted into kinetic energy. In Chapter 11, a slider-block model is used to describe the kinematics of this earthquake process. This model consists of a block of mass M, which is driven by a constant-velocity driver at speed V until the force, kx, on a spring exceeds the static friction force. An equation of motion, which applies once sliding has begun, is used to describe the time evolution of the system. Single-block solutions provide the foundation for the more 'Earth-like' two-block analyses that are also discussed in the text. It is in these latter analyses that the signs of chaos can be well illustrated, and promising comparisons with real earthquake data can be made.

In his classic article (*Deterministic Nonperiodic Flow*, J. Atmos Sci., 20, 130-141, 1963) E. N. Lorenz essentially 'discovered' what we now refer to as chaos, i.e. an exponential sensitivity to initial conditions. Lorenz was interested in the study of thermal convection in a fluid layer heated from below. In Chapter 12 a thorough review of Lorenz's problem, which involves a set of three coupled total differential equations, is provided. The author provides the details for the derivation of the Lorenz system, the calculation of the system's evolution, and projections of the resulting Lorenz attractor. In the following chapter, the author uses the formalism developed for the Lorenz problem to investigate the nature of thermal convection in the Earth's mantle. Using a double Fourier series expansion and scalings appropriate to mantle convection, the author illustrates the chaotic nature of this hydrodynamic instability. In Chapter 14, a numerical solution of the Rikitake two-disk dynamo equations is shown to have some properties in common with the solution of the Lorenz equations, and possess some similarities to actual sequences of magnetic field reversals recorded over geologic time scales.

The last two chapters, which precede the very brief concluding chapter, are concerned with large interactive systems. In Chapter 15, the renormalization group method is applied to fluid flow in a porous medium, fragmentation, and a fractal tree model for rupture of a fault. Self-organized criticality is used to re-investigate the earthquake frequency-size distribution problem, and seems to show some predictive promise.

This is a purposefully, concisely, and well-written book on an important formalism for geology and geophysics. It is fortunate that someone with the author's experience and stature has taken the time to put together this impressive synthesis. Despite its relatively small length, this book spans many interesting topics and is completely self-contained. It would thus be highly suitable as a senior undergraduate or graduate-level text. Although the overall organization of the text is satisfactory, chapter subheadings would be a welcome addition.

Those interested in this subject might also want to examine the monograph *Nonlinear Dynamics and Predictability of Geophysical Phenomena,* Geophysical Monograph 83, American Geophysical Union, 1994, which is co-edited by this same author.

Ian Lumb, Research Scientist
KelResearch Corporation
Consultants in Atmospheric Science & Technology
850-A Alness Street, Suite 9
Downsview, Ontario M3J 2H5 CANADA
Voice: 416-736-0521; FAX: 416-661-7171
Internet: <kel@nexus.yorku.ca>

"Chaos In Wonderland", A Book By Clifford Pickover

From the publisher's release:

"*Alice in Wonderland* meets *2001: A Space Odyssey!*

"Stir together a mixture of fractals, chaos, computer graphics, and science fiction. What do you get? You get a dazzling introduction to chaos science by Clifford Pickover, IBM's indefatigable computer scientist. Dr. Pickover alleges that his gorgeous swirling art, generated by the strange attractors of two simple formulas are the dreams of limbless, brainy creatures living below the icy surface of Ganymede, Jupiter's largest moon.

""Things flow about here!' exclaimed Alice, in the queer little shop behind the mirror; but never in Lewis Carroll's wildest imagination could she have dreamed of the flowing patters in Pickover's Wonderland."

—Martin Gardner, *Scientific American*

"A fascinating project, a worthy addition to *Flatland* and *The Planiverse!*'

—Arthur C. Clarke

"Pickover weaves a fascinating and entertaining tale of fact and fiction in *Chaos in Wonderland.* While learning of the intricacies of the world of the Latoeoecarfians, we are skilfully introduced to the mathematics of chaos. His mixture of fantasy and mathematics creates an eeriness of reality that is both informative and thought provoking."

—Theoni Pappas, author of *The Joy of Mathematics*

"A leading expert in computer visualization, Pickover now enthralls us with his art, mathematical games, and science fiction. This latter-day Lewis Carroll introduces us to alien creatures with computer brains and mathematical souls. Their social status is based on the beauty of geometrical patterns communicated to one another with infrared beams. You will be delighted at the mathematical wonderland Pickover provides using media more suited to us humans.

—Prof. J.C. Sprott, author of *Strange Attractors*

"Chaos Under Control"

—A.G. Davis Philip

I have before me a recently published book, "Chaos Under Control, The Art and Science of Complexity" by David Peak and Michael Frame of Union College. A short summary of the contents can be given by listing the subjects of the ten chapters:

1. Introduction — why chaos and fractals are interesting
2. Iterated Function Systems
3. Fractal Dimensions
4. Chaotic Dynamics and Graphical Iteration
5. Order in Chaotic Dynamics —Bifurcation Diagrams
6. Graphical Test of Chaos
7. Mandelbrot set and Julia sets
8. Fractal Basin Boundaries
9. Cellular Automata, Neural Nets, Sandpiles and Artificial Life
10. Fractals and Chaos in the Humanities and Social Sciences.

There are 16 color plates in the center of the book., which is now being used in courses at Union College, Yale University and the University of Richmond. In a foreword by Mandelbrot, he writes, "The observation is that fractals — together with chaos, easy graphics and the computer — enchant many young people, which — in turn — makes them excited about learning mathematics and physics.... In this book David Peak and Michael Frame have taken a step in realizing this hope."

"Fractal Cities"

—Michael Batty and Paul Longley

From the publishers description:

Fractal Cities is a study of the development and use of fractal geometry for understanding and planning the physical form of cities, showing how this

geometry enables cities to be simulated through computer graphics. It shows how cities evolve and grow in ways that at first sight appear irregular, but which, when understood in terms of fractals, illustrate an underlying order that reveals their complexity and diversity.

The book contains sixteen pages of computer graphics and explanations of how to construct them, as well as new insights into the complexity of social systems. The authors provide an intelligible and gentle introduction to fractal geometry as well as an exciting visual understanding of the form of cities, thus providing one of the best introductions to fractal geometry available for non-mathematicians and social scientists.

Fractal Cities can be used as a text for courses on geographic information systems, urban geography, regional science and fractal geometry. Planners and architects will also find that there are many aspects of fractal geometry in this book relevant to their own interests. Furthermore, those involved in fractals and chaos, computer graphics and systems theory will find important methods and examples which are germane to their work.

Michael Batty is Director of the National Center for Geographic Information and Analysis in the State University of New York at Buffalo, and Paul Longley is Reader in Geography at the University of Bristol.

Book Reviews Wanted

If you run across a book on the subject of fractals, etc. that seems particularly illuminating, and has not yet been reviewed in Amygdala, think about writing a review of the book and sending it in for possible publication in Amygdala.

Quaternion Square Root

Rollo Silver

This note on quaternion arithmetic arose in response to a question posed by Bill Bell on the Internet FRAC-L forum. He wrote, "I'm trying to write a program to display 3-D Julia sets using quaternions. My problem is, the math still baffles me a little bit, in particular trying to figure out how to calculate the square root of a quaternion. I've looked up most of the magazine articles treating this subject, but their explanations are still not penetrating my thick skull. I keep winding up trying to find the arctangent of a complex number, which I'm not sure is possible."

I worked out a simple algorithm for the square root of a quaternion, not involving anything as complicated as the arctangent of a complex number. Gerald Edgar pointed out errors in my first two attempts to get the algorithm right— Now I think it's right!

So here we go, computing the quaternion r which is the square root $r = \sqrt{q}$ of a quaternion q.

Let

$$q = q_0 + iq_1 + jq_2 + kq_3 \qquad [6]$$

and let

$$r = r_0 + ir_1 + jr_2 + kr_3 \qquad [7]$$

be a root of

$$r^2 = q \qquad [8]$$

In summary we have:

(1) If $q = 0$, then [8] has precisely one root: $r = 0$.

(2) If q is negative real, then [8] has an infinity of roots [7] with $r_0 = 0$ and $r_1^2 + r_2^2 + r_3^2 = -q_0$.

(3) Otherwise [8] has precisely two roots,

$$r = \pm\left(\rho + \frac{iq_1}{2\rho} + \frac{jq_2}{2\rho} + \frac{kq_3}{2\rho}\right), \text{ where}$$

$$\rho = \sqrt{\frac{q_0 + \sqrt{q_0^2 + q_1^2 + q_2^2 + q_3^2}}{2}}.$$

Now for the gory details.

From [7] we have

$r^2 = (r_0 + ir_1 + jr_2 + kr_3)(r_0 + ir_1 + jr_2 + kr_3)$,

which expands and simplifies to

$$r^2 = r_0^2 - r_1^2 - r_2^2 - r_3^2 + 2ir_1r_0 + 2jr_2r_0 + 2kr_3r_0 \quad [9]$$

Substituting [9] and [6] in [8], we get

$r_0^2 - r_1^2 - r_2^2 - r_3^2 + 2ir_0r_1 + 2jr_0r_2 + 2kr_0r_3 =$

$q_0 + iq_1 + jq_2 + kq_3$. Equating the four quaternion components separately, we get:

$$r_0^2 - r_1^2 - r_2^2 - r_3^2 = q_0 \quad [10]$$

and

$$2r_1r_0 = q_1 \,,\; 2r_2r_0 = q_2 \,,\; 2r_3r_0 = q_3 \quad [11]$$

Our task is to find all real r_0, r_1, r_2, r_3 which satisfy [10] and [11].

Case 1: q is real.

That is, $q = q_0$. We have two subcases, $r_0 = 0$ and $r_0 \neq 0$.

Case 1.1: q is real ($q = q_0$) and $r_0 = 0$.

From [10], $r_1^2 + r_2^2 + r_3^2 = -q_0$, and so $q_0 \leq 0$, and *any* r_1, r_2, r_3 satisfying $r_1^2 + r_2^2 + r_3^2 = -q_0$ define a root $r = ir_1 + jr_2 + kr_3$ of [8]. For example, if $q = -1$, the following are among the infinity of roots of [8]: $i, j, k, \frac{i+j+k}{\sqrt{3}}$.

Case 1.2: q is real ($q = q_0$) and $r_0 \neq 0$.

Since $r_0 \neq 0$, while each of q_1, q_2, q_3 is 0 (since q is real), [11] implies that $r_1 = r_2 = r_3 = 0$, in which case [8] reduces to $r_0^2 = q_0$. We must have $q_0 \geq 0$, and [8] has either one or two roots, depending on whether $q_0 = 0$ or $q_0 > 0$. If $q = 0$ then $r = 0$. If $q > 0$ then $r = \pm\sqrt{q}$.

Case 2: q is not (pure) real; i.e. not all of q_1, q_2, q_3 are zero.

In this case $r_0 \neq 0$, lest by [11], $q_1 = 0$, $q_2 = 0$, $q_3 = 0$. We can then divide each of the equations [11] by r_0 and get

$$r_1 = \frac{q_1}{2r_0} \,,\; r_2 = \frac{q_2}{2r_0} \,,\; r_3 = \frac{q_3}{2r_0} \quad [12]$$

Substituting [12] in [10]:

$r_0^2 - \left(\frac{q_1}{2r_0}\right)^2 - \left(\frac{q_2}{2r_0}\right)^2 - \left(\frac{q_3}{2r_0}\right)^2 = q_0$, or

$4r_0^4 - 4q_0r_0^2 - (q_1^2 + q_2^2 + q_3^2) = 0$, whose roots are

$r_0^2 = \frac{q_0 \pm \sqrt{q_0^2 + q_1^2 + q_2^2 + q_3^2}}{2}$. Since r_0 is real and nonzero, $r_0^2 > 0$. But $q_0^2 < q_0^2 + q_1^2 + q_2^2 + q_3^2$, so we must take the sign of the square root to be positive:

$$r_0^2 = \frac{q_0 + \sqrt{q_0^2 + q_1^2 + q_2^2 + q_3^2}}{2} \,, \quad [13]$$

We have ρ and $-\rho$ as solutions of [13], where

$$\rho = \sqrt{\frac{q_0 + \sqrt{q_0^2 + q_1^2 + q_2^2 + q_3^2}}{2}} \quad [14]$$

Applying [7] and [12], in this case [8] has precisely two roots:

$$r = \pm\left(\rho + \frac{iq_1}{2\rho} + \frac{jq_2}{2\rho} + \frac{kq_3}{2\rho}\right) \quad [15]$$

Authors

Gabriel Landini received a Dental degree (DDS) from Uruguay University in 1984 and a Ph.D in Oral Pathology from Kagoshima University, Japan in 1991. At the present time he works at Birmingham University on several applications of fractal geometry to the medical sciences.

Address: 87 Tenby Road, Moseley, Birmingham B13 9LT, England.

Lee H. Skinner works as a senior computer analyst at Sandia National Laboratories in Albuquerque, N.M. Fractals have been his hobby for the last five years; he uses FractInt on a 486 DX4 computer.

Among his other interests are math games, chess, Go, and hiking.

Ian Lumb's research efforts are geared towards the completion of his Ph.D. degree in Physics and Astronomy at York University (North York, Ontario, Canada), and towards several contracts at the KelResearch Corporation (Downsview, Ontario, Canada). It was at KelResearch that he first had the opportunity to delve into the depths chaos and fractals, and continues to study image processing and analysis via fractal-based methods. Ian also teaches at York University and is an avid Internetworker. He is married with three daughters.

Each One Bring One

Subscribers, I need your help! The more Amygdala subscribers we have, the better the newsletter will be!

I have been working to build circulation by posting notices on Internet forums and newsgroups, and on Compuserve forums, but I need your help! Please reach out among your friends, acquaintances, coworkers, etc. to sign up new subscribers for Amygdala.

The subscription rates for ten issues are $28.20 (US), $32.00 (Canada & Mexico), $39.00 (Other). First Class or Air Mail postage included.

We also need material for future issues! My writing takes the lion's share of this issue, and I think that we need more diversity. If you can write, and have material that you think would interest Amygdala readers, please submit it for publication. See the **Submitting Articles** guidelines on this page.

Amygdala is published by Rollo Silver every eight to ten weeks.

Address articles, letters, comments, subscription orders, to: *Amygdala; Box 219; San Cristobal, NM 87564; USA.*

Email: rsilver@beta.lanl.gov
Phone/FAX: 505/586-0197
Compuserve: 71174,1453

This issue was produced using FrameMaker on a Macintosh IIcx computer.

Submitting Articles

Here are some guidelines for submitting articles for publication in Amygdala.

1. Type your article as you would like to see it appear in the newsletter. Please do not send handwritten drafts!

Send it (*my* order of preference): (A) On 3.5" diskette in Macintosh format for FrameMaker, MacWrite, WriteNow, or MS Word; or as a text file. Please also enclose paper copy so I can see your intent. (B) On 3.5" diskette in IBM format, text file. I have no way to deal with 5.25" diskettes. (C) Paper copy.

2. Illustrations should be either greyscale (suitable for halftoning) or black/white; not color! (A) Normally, illustrations will be printed in full column width, so you should make them 3.25" wide, if possible — provided that they're 300 dpi resolution. If they're grainier, make them larger if possible, so that they'll look good when reduced to 300 dpi. (B) Make sure that you clearly indicate which illustrations go where in the text! (C) All in all, it's better not to have captions welded into your pictures. Let me put them in ad lib. (D) I can handle illustrations on diskette in MacPaint, MacDraw, CricketDraw, Photoshop, or Adobe Illustrator formats.

3. Please send along a short biographical note, which I will try to publish in the same issue as your article.

4. Please include your telephone number, in case I have to reach you in a hurry with questions.

Circulation/Renewal

As of October 29, 1994, Amygdala has 438 subscribers.

The address used for mailing this issue to you has a small notation at the lower right indicating when your subscription expires.

A33 or *A34* indicates that this is your last issue. *A35* or*A36* indicates that your subscription expires with the next issue. In either case, please use the form on the other side of the address page to renew.